

Charge-Transfer-Induced Cesium Superlattices on Graphene

Can-Li Song,^{1,2} Bo Sun,³ Yi-Lin Wang,¹ Ye-Ping Jiang,^{1,2} Lili Wang,¹ Ke He,¹ Xi Chen,² Ping Zhang,³
Xu-Cun Ma,^{1,*} and Qi-Kun Xue^{1,2,*}

¹Beijing National Laboratory for Condensed Matter Physics, Institute of Physics, Chinese Academy of Sciences,
Beijing 100190, China

²State Key Laboratory of Low-Dimensional Quantum Physics, Department of Physics, Tsinghua University, Beijing 100084, China

³Institute of Applied Physics and Computational Mathematics, Beijing 100088, China

(Received 24 August 2011; published 11 April 2012)

We investigate cesium (Cs) adsorption on graphene formed on a 6H-SiC(0001) substrate by a combined scanning tunneling microscopy and density functional theory study. Individual Cs atoms adsorb preferentially at the rim region of the well-defined 6×6 substrate superstructure and on multilayer graphene. By finely controlling the graphene thickness and Cs coverages (1/3 ML and 1 ML), we here demonstrate two intriguing and well-ordered Cs superlattices on bilayer and multilayer graphene (< 6 layers). Statistical analysis of the Cs-Cs interatomic distance reveals a hitherto unobserved Cs-Cs long-range electrostatic potential caused by charge transfer from Cs to graphene, which couples with the inhomogeneous substrate potential to stabilize the observed Cs superlattices. The present study provides a new avenue to fabricate atomic and molecular superlattices for applications in high-density recording and data storage.

DOI: 10.1103/PhysRevLett.108.156803

PACS numbers: 73.22.Pr, 68.37.Ef, 71.15.Mb, 78.67.Pt

Understanding the unique interactions of atoms and molecules on an atomically well-defined surface and then controlling their assembly structures is a promising route to build future device applications with nanometer dimensions. Previous studies have demonstrated that atoms and molecules adsorbed on a solid surface can interact with each other indirectly *via* electron scattering or elastic distortion of the substrate [1–6]. Such substrate-mediated long-range interatomic or intermolecular interactions appear to play a significant role in the atomic and molecular assembly. Typical examples include the creation of well-ordered Ce atomic superlattice on Ag (111) surface by Silly *et al.* [2,3] and equilateral metal nanostructures on strained substrates by Brune *et al.* [5]. However, thus far, most experimental studies have been devoted to metal surface [1–5], which limits certain device applications to great extent. An alternative choice is to explore similar studies on graphene, which represents a star material in the next generation of high-performance devices [7]. Despite intense experimental and theoretical endeavors on adsorbates-graphene systems [8–15], almost all studies focus on either the adsorbate-graphene interactions or the modified graphene properties upon atom and molecule adsorption [8–14], leaving the interactions between adsorbates rarely touched [15].

In this Letter, we report our scanning tunneling microscopy (STM) study of cesium (Cs) adsorption behaviors, Cs-graphene and Cs-Cs interactions on epitaxial graphene (EG) formed on Si-polar 6H-SiC(0001) substrate. We show that adsorption of Cs atoms critically depends on the layer number of graphene, and they preferentially occupy on multilayer EG and then at rim sites of the 6×6 superstructure of monolayer EG (MEG). At moderate

coverages (1/3 ML and 1 ML), Cs spontaneously assembles into two long-range ordered superlattices on bilayer EG (BEG) as well as multilayer EG (< 6 layers) with a peculiar period of 1.85 and 3.20 nm, respectively. By extracting Cs-Cs pair-distance distributions at various coverages, an interatomic Coulomb repulsion potential due to the charge transfer from Cs to graphene is unambiguously revealed, excellently consistent with our density functional theory (DFT) calculations. The observed superlattices are cooperatively stabilized by this long-range Coulomb repulsive force and the inhomogeneous substrate potential.

Our experiments were performed using an ultrahigh vacuum low-temperature STM apparatus (Unisoku) with a base pressure of 5×10^{-11} Torr. EG was thermally prepared on a commercially nitrogen-doped 6H-SiC(0001) wafer with a resistivity of $\sim 0.1 \Omega \cdot \text{cm}$ [16]. Depending on the temperature (1300 °C–1500 °C) and duration of the thermal treatment, MEG, BEG and multilayer EG can be easily obtained on the SiC substrate. Cs atoms were then evaporated from a thoroughly outgassed getter source (SAES) onto the substrate cooled down to 150 K by liquid nitrogen. It was found that Cs atoms rapidly desorb from the graphene at a slightly higher temperature of 200 K. The Cs coverages we studied range from 0.04 ML to 1.5 ML (here 1 ML is defined as one adatom per 6×6 superstructure unit cell, $\sim 3.4 \times 10^{13}/\text{cm}^2$). Upon deposition, the samples were immediately transferred to the STM stage for data collections at 4.8 K by using polycrystalline W tips. The *ab initio* DFT calculations were carried out using the VASP code with the local density approximation and projector-augmented wave pseudopotential [17]. The chosen supercell with more than 2000 atoms consists of the hydrogen passivated 6H-SiC(0001) substrate, the 13×13

buffer layer followed by the EG, and a vacuum spacing of 25 Å. The geometry optimization is carried out until the forces on all atoms are less than 0.01 eV/Å. The plane-wave cutoff energy of 400 eV is applied, and during self-consistent calculations the total-energy convergence is set to be within 0.001 eV.

Figure 1(a) shows a 5 nm × 5 nm topographic image of MEG. It exhibits a well-identified honeycomb lattice of the graphene superimposed onto the 6 × 6 corrugation background (white hexagon). It turns out that the 6 × 6 pattern even appears on multilayer EG albeit with reduced contrast. The pattern has a periodicity of 1.85 nm and originates from the underlying $6\sqrt{3} \times 6\sqrt{3}R30^\circ$ reconstruction of the buffer layer, which commonly appears as a reduced 6 × 6 periodicity in high-bias STM images of 6H-SiC (0001) [18,19]. As illustrated in Fig. 1(a), the 6 × 6 superstructure contains two distinctive regions: the lattice matched region (valley) and lattice mismatched region (rim), where the carbon atoms in the buffer layer are alternatively bonded and not bonded to the Si atoms in the top SiC layer, respectively [18]. The contrast variation between valley (minimum) and rim (maximum) is strongly bias dependent and typically ~60 pm at 30 mV.

Upon Cs deposition, identical protrusions of approximately 0.5 nm in height are observed, as exemplified in both Figs. 1(b) and 1(c). They are explained as single Cs

adatoms. Interestingly, the density of Cs adatoms is substantially affected by the number of graphene layers. For each Cs coverage investigated, the population of adsorbed Cs increases with the number of graphene layers, e.g. BEG > MEG [Fig. 1(b)]. This shows great resemblance to the case of lithium [12], suggesting the weakest interaction between Cs and MEG. A closer examination of the STM image reveals that Cs atoms exhibit a strong tendency to adsorb at the rim region of the 6 × 6 superstructure. For example, in Fig. 1(c) six out of seven Cs adatoms are positioned at the rims, like hydrogen [19]. This is more clearly verified in the statistical analysis of Cs adsorption sites within the 6 × 6 superstructure [Fig. 1(d)], which was obtained by sampling roughly 500 Cs adatoms. More than 95% Cs decorate the rim regions on MEG. Our *ab initio* calculations also support this observation. According to our calculations, a difference of ~50 meV in the binding energy (ΔE_b) for Cs at the rim and valley regions develops on MEG. In the case of Cs on BEG, the binding energy difference ΔE_b sharply reduces to ~15 meV. Thus, the preferential adsorption is significantly decreased, as well confirmed in Fig. 1(d). This phenomenon can be most likely account for by the curvature effect, which changes noticeably the chemical activity and binding energy of graphene [19–21]. Large surface curvature, such as the rim regions, often represents energetically favorable binding sites. Therefore, one can expect that Cs atoms should preferentially adsorb at the rim regions, as observed above.

We further investigate the Cs adsorption behaviors on MEG and BEG at various Cs coverages. As discussed above, Cs atoms prefer the rim region of the 6 × 6 superstructure. Thus if 1 ML Cs atoms are deposited on MEG and most atoms will occupy at the rim regions, a hexagonal superlattice with a periodicity of 1.85 nm can be naturally expected. However, contrary to this speculation, only a short-range ordered hexagonal structure with an average interadatom separation of 1.85 nm is found [Fig. 2(a)]. Instead the expected superlattice occurs on BEG quite unexpectedly, as shown in Fig. 2(b) and the corresponding 2D power spectrum (inset). Here six sharp spots, the signal of well-ordered superlattice, markedly differ from the blurred weak spots and ring structure in the inset of Fig. 2(a), suggestive of the absence of long-range order of Cs adatoms on MEG.

Additionally, at a lower coverage (~1/3 ML), Cs atoms even self-organize into another long-range ordered superstructure with a period of ~3.20 nm on BEG [Fig. 2(c)]. Note that 3.20 nm is $\sqrt{3}$ times the period of the 6 × 6 superstructure. For convenience, the structures in Figs. 2(b) and 2(c) are referred as 1 × 1 and $\sqrt{3} \times \sqrt{3}$ superlattices hereafter, respectively. The 1 × 1 superlattice can be stable up to 80 K, the highest observation temperature available in our experiment (cooled down by liquid helium). In contrast, the $\sqrt{3} \times \sqrt{3}$ superlattice only stabilizes below 9 K. Above this temperature, Cs adatoms

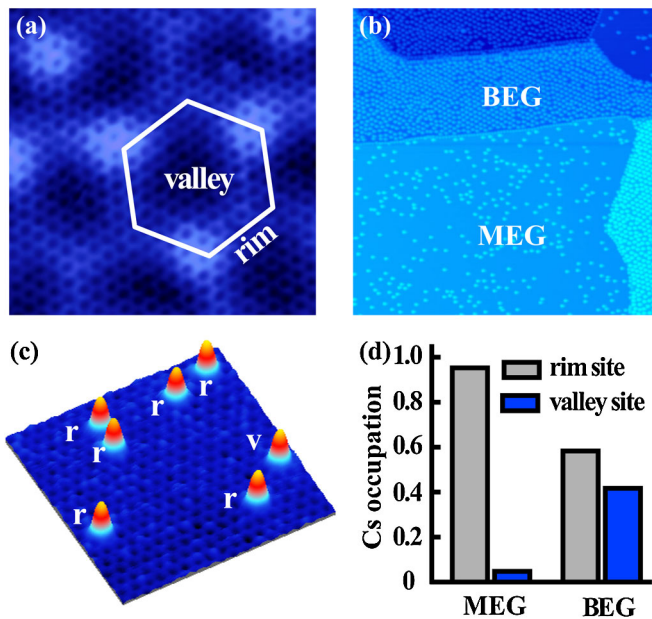


FIG. 1 (color online). (a) Atomically resolved STM image (5 nm × 5 nm) of MEG on SiC(0001). Imaging conditions: $V_s = 30$ mV, $I = 0.1$ nA. (b) STM image of Cs adatoms on MEG and BEG (200 nm × 200 nm, $V_s = 2.0$ V, $I = 0.1$ nA). (c) Three-dimensional STM image of ~0.04 ML Cs adsorbed on MEG (30 nm × 30 nm, $V_s = 4.2$ V, $I = 0.1$ nA). (d) Histograms showing site-dependent Cs occupation probabilities within the 6 × 6 superstructure for MEG and BEG, respectively. Each histogram involves roughly 500 adatoms.

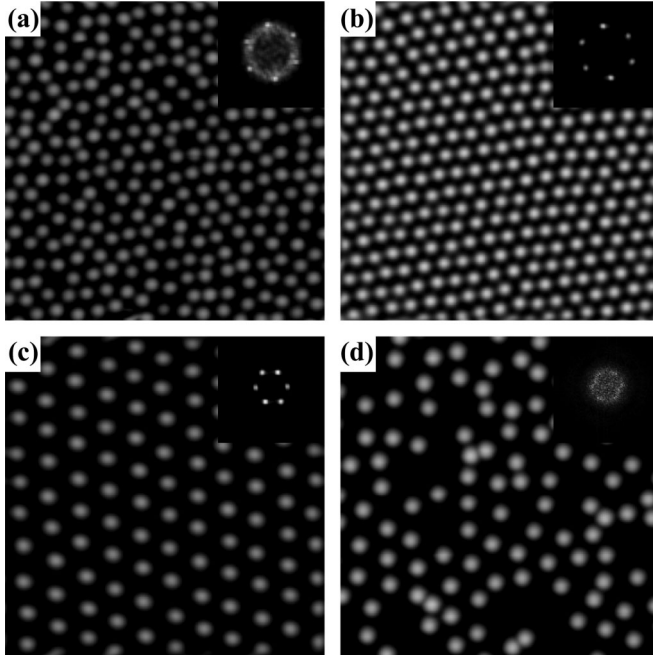


FIG. 2. STM images ($30 \text{ nm} \times 30 \text{ nm}$) of (a) 1 ML Cs adsorbed on MEG ($V_s = 1.5 \text{ V}$, $I = 0.1 \text{ nA}$); (b) 1 ML Cs adsorbed on BEG ($V_s = 1.0 \text{ V}$, $I = 0.1 \text{ nA}$); (c) 1/3 ML Cs adsorbed on BEG ($V_s = 1.0 \text{ V}$, $I = 0.05 \text{ nA}$); and (d) 1/3 ML Cs adsorbed on 6 layers EG ($V_s = 1.5 \text{ V}$, $I = 0.06 \text{ nA}$). Insets display the corresponding power spectra.

becomes quite disordered. Moreover, both the 1×1 and $\sqrt{3} \times \sqrt{3}$ superlattices can also occur on multilayer EG as long as the number of graphene layers does not exceed five. As illustrated in Fig. 2(d), when the layer number increases to six, Cs adatoms do not form any ordered structure although the coverage is the same as that in Fig. 2(c).

The long-range-ordered Cs superlattices on BEG and few-layers EG (< 6 layers) cannot phenomenologically be explained by the template effect of the 6×6 superstructure [22,23], because they do not occur on MEG where the template effect should be the strongest. To find out the formation mechanism, we conduct an analysis on the interactions between Cs adatoms. Figure 3 shows the nearest-neighboring (NN) Cs-Cs interadatom occupation probability histograms $f(r)$ at various Cs coverages on both MEG and BEG. More than 3000 pairs were counted for each plot with \bar{r} indicating the average pair distance. In terms of the two-body interactions, the probability distribution $f(r)$ modulated by the interadatom potential $E(r)$ can be written as

$$f(r) = f_{\text{ran}}(r) \times \exp\{-[E(r) - \mu]/k_B T\}, \quad (1)$$

where k_B is the Boltzmann constant, r is the Cs-Cs NN separations, μ is coverage-dependent zeroth order chemical potential and $f_{\text{ran}}(r)$ is the noninteracting adatom random separation distribution [1]. In a two-dimensional

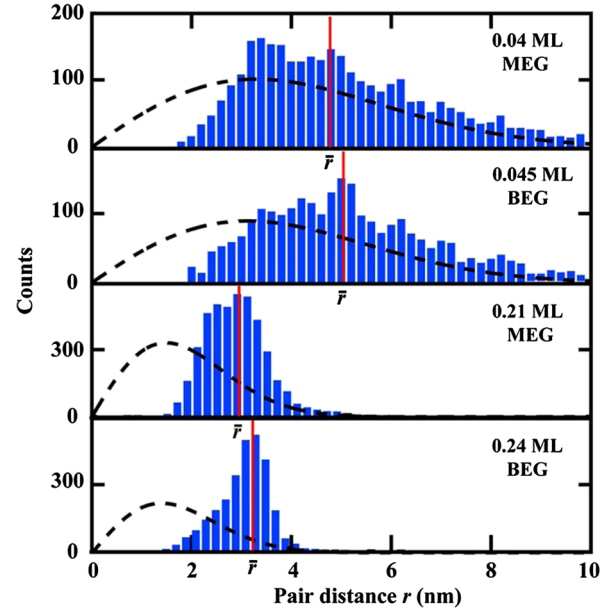


FIG. 3 (color online). Histograms of the nearest-neighboring pair-distance and random distributions (black dashed lines) for noninteracting adatoms at various Cs densities on MEG and BEG. For each plot, ~ 3000 pairs are analyzed. From the top to the bottom panel, an average pair distance \bar{r} is identified as 4.8, 5.0, 2.9, 3.1 nm, respectively.

system, $f_{\text{ran}}(r)$ is coverage-dependent and shows a peaked distribution as a function of the separation r , as indicated by the dashed lines in Fig. 3. Compared with the probability peak positions in $f_{\text{ran}}(r)$, \bar{r} obviously shifts towards larger value, particularly at high Cs coverages and on BEG. For example, \bar{r} is 3.1 nm on BEG (0.24 ML), which is larger than 2.9 nm on MEG (0.21 ML), even the Cs coverage on BEG is a little bit higher than that on MEG. These observations strongly suggest the occurrence of long-range repulsive interactions between Cs adatoms, and it appears stronger on BEG.

To clarify the nature of the repulsive interactions, we have quantitatively evaluated the interadatom repulsive potential $E(r)$ from Eq. (1). Figure 4 shows the deduced potential curves at various Cs coverages on BEG. Here, $E(r)$ does not exhibit a monotonic behavior, rather, a minimum at certain points. Departing from the points, the potential will increase. This can be easily understood in terms of the strong interadatom repulsive interactions. For two-dimensional particle system with repulsive interactions, the ground state with minimum interaction energy will be that all particles assembly into a well-ordered superstructure. Any small perturbation in particle ordering will increase the system energy, leading to the nonmonotonic behavior. With increasing Cs coverage, the minimum shifts to smaller distance and the potential increases more quickly at larger distance. By a careful comparison with various decay functions, we find that $E(r)$ decays as $\sim 1/r$ at small distance, suggesting that the dominating

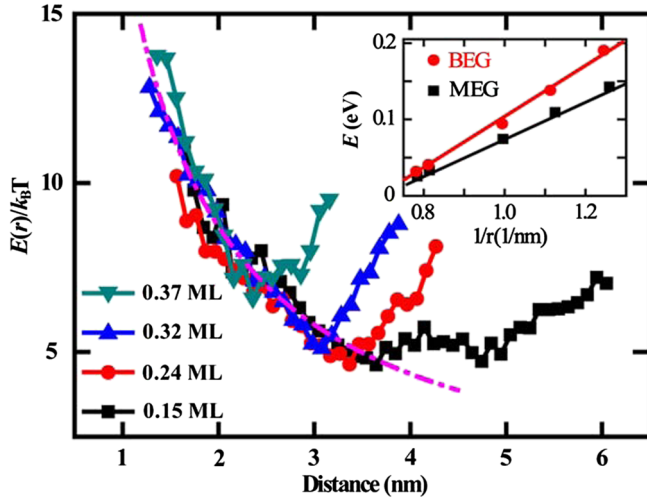


FIG. 4 (color online). Mean interaction potential of Cs adatoms on BEG extracted from the pair distribution in Fig. 3. Each curve has been shifted upwards an amount (5.7, 7.1, 8.1, 9.4 from the lowest to the largest coverage) in charge of the coverage-dependent zeroth order internal potential. An electrostatic potential between particles charged with 0.4 e (dashed line, $T = 150$ K) shows the best fit to the data at small pair distances. Inset: *Ab initio* calculated Cs-Cs interaction energy on MEG and BEG as a function of $1/r$. The straight lines are to guide the eyes.

interactions between Cs adatoms are electrostatic. We further find that an electrostatic potential among particles charged with 0.4 e (dashed line in Fig. 4, $T = 150$ K) shows the best fit to the data at small distances. This $1/r$ decay radically discriminates from the exceptionally rapid decay of $1/r^3$ for Cs adsorbed on graphite as well as metal surface due to dipole-dipole interactions [24,25]. Here the difference in decay behavior possibly suggests a weaker electron screening effect in graphene than in graphite as well as metal surface [26]. The same $1/r$ decay behavior is also found on MEG, where each Cs adatom transfers ~ 0.33 e into MEG. More charge transfer means larger adsorption energy and stronger repulsive interactions between Cs adatoms, as evidenced above.

Indeed, Cs atoms are observed to donate their electrons to graphene. dI/dV spectra of BEG before and after 0.45 ML Cs adsorption reveal that the Fermi level shifts upward from 0.38 to 0.47 eV with respect to the Dirac point (not shown). This corresponds to nearly 0.38 e charge transfer per Cs, consistent with the fitting result above. The inset of Fig. 4 shows our *ab initio* calculation of the Cs interaction energy as a function of $1/r$. Perfect linearity between E and $1/r$ corroborates the coulomb repulsion between Cs adatoms. Clearly, a larger slope appears on BEG, suggesting more prominent charging and repulsive forces of Cs on BEG.

The long-range surface-state mediated adatom interactions were previously shown to result into well-ordered Cerium superlattices on Ag(111) [2,3]. In our case,

however, the nonoscillatory behavior in pair-distance distribution and $E(r)$ exclude this possibility. In terms of the $1/r$ decay of the repulsion potential, the $1/r^3$ elastic potential mediated by the distortion of the substrate also appears to be safely ruled out [6]. Furthermore, if it indeed works, the superstructure should have occurred more easily on MEG with the strongest elastic potential, which is inconsistent with our experiment.

Therefore, we propose that both the corrugated graphene due to the 6×6 superstructure and the substrate-mediated repulsive Coulomb interaction play roles in the formation of Cs superlattices. The former acts as a template for Cs nucleation in terms of the preferential Cs adsorption at the rim regions. The energy barrier between rim and valley sites restricts the surface diffusion and so appears essential for the stabilization of the Cs superlattices. Without this effect, the period of superstructure may not be necessarily 1.85 nm (1×1) and 3.20 nm ($\sqrt{3} \times \sqrt{3}$) and small thermal perturbation or coverage fluctuation will severely destroy the superlattices. Meanwhile, the roles played by the substrate-mediated interadatom repulsive Coulomb interaction are twofold. One is to prevent dimer or cluster formation, which tend to significantly degrade the superlattice. In our case, this is always satisfied because of strong electrostatic repulsion between charged Cs adatoms (little dimer or cluster is found even when the Cs coverage exceeds 1 ML). The other role is to stabilize the superlattice. Generally speaking, strong electrostatic repulsion often corresponds to high stability against perturbations. In Cs/MEG system, despite large surface corrugations, the electrostatic repulsion between charged Cs adatoms is not strong enough to stabilize the long-range ordering of Cs superlattice [Fig. 2(a)]. On the other hand, for Cs adsorbed on multilayer EG (> 5 layers), the electrostatic repulsion may be strong enough, but the graphene surface is thus flat that small thermal perturbation will lead Cs to distribute on multilayer EG randomly. As a consequence, the long-range superlattice cannot also form [Fig. 2(d)]. Only on EG with intermediate layers (2–5 layers), Cs superlattices self-form [Figs. 2(b) and 2(c)] since both substrate corrugation and electrostatic repulsion are appropriately strong for the formation of Cs superlattices. Such a model predicts that the stabilization of the superlattices is extremely sensitive to adatom diffusion barrier, sample temperature, Cs coverage and the electrostatic repulsion between charged Cs adatoms, quite in line with our experiments.

In summary, we have demonstrated a long-range repulsive Coulomb potential between Cs adatoms adsorbed on graphene formed on 6H-SiC(0001), which originates from the charge transfer from Cs to graphene. The formation of Cs superlattices results from the combination of the inhomogeneous substrate potential and repulsive Coulomb potential between Cs adatoms. We anticipate that the identified approach can be utilized to design other atomic and molecular superlattices on graphene.

Acknowledgements: This work was supported by National Science Foundation and Ministry of Science and Technology of China. All STM topographic images were processed by WSxM software (www.nanotec.es).

*Corresponding authors.

xcma@aphy.iphy.ac.cn

qkxue@mail.tsinghua.edu.cn

- [1] N. Knorr, H. Brune, M. Epple, A. Hirstein, M. A. Schneider, and K. Kern, *Phys. Rev. B* **65**, 115420 (2002).
- [2] F. Silly, M. Pivetta, M. Ternes, F. Patthey, J. P. Pelz, and W.-D. Schneider, *Phys. Rev. Lett.* **92**, 016101 (2004).
- [3] F. Silly, M. Pivetta, M. Ternes, F. Patthey, J. P. Pelz, and W.-D. Schneider, *New J. Phys.* **6**, 16 (2004).
- [4] T. Yokoyama, T. Takahashi, K. Shinozaki, and M. Okamoto, *Phys. Rev. Lett.* **98**, 206102 (2007).
- [5] H. Brune, M. Giovannini, K. Bromann, and K. Kern, *Nature (London)* **394**, 451 (1998).
- [6] K. H. Lau, *Solid State Commun.* **28**, 757 (1978).
- [7] K. Kim, J.-Y. Choi, T. Kim, S.-H. Cho, and H.-J. Chung, *Nature (London)* **479**, 338 (2011).
- [8] G. Giovannetti, P. A. Khomyakov, G. Brocks, V. M. Karpan, J. van den Brink, and P. J. Kelly, *Phys. Rev. Lett.* **101**, 026803 (2008).
- [9] H. Q. Zhou, C. Qiu, Z. Liu, H. Yang, L. Hu, J. Liu, H. Yang, C. Gu, and L. Sun, *J. Am. Chem. Soc.* **132**, 944 (2010).
- [10] J. Lee, K. S. Novoselov, and H. S. Shin, *ACS Nano* **5**, 608 (2011).
- [11] E. Pollak, B. Geng, K.-J. Jeon, I. T. Lucas, T. J. Richardson, F. Wang, and R. Kostecki, *Nano Lett.* **10**, 3386 (2010).
- [12] T. Ohta, A. Bostwick, T. Seyller, K. Horn, and E. Rotenberg, *Science* **313**, 951 (2006).
- [13] M. Khantha, N. A. Cordero, L. M. Molina, J. A. Alonso, and L. A. Girifalco, *Phys. Rev. B* **70**, 125422 (2004).
- [14] K. H. Jin, S. M. Choi, and S. H. Jhi, *Phys. Rev. B* **82**, 033414 (2010).
- [15] A. V. Shytov, D. A. Abanin, and L. S. Levitov, *Phys. Rev. Lett.* **103**, 016806 (2009).
- [16] P. Lauffer, K. V. Emtsev, R. Graupner, Th. Seyller, L. Ley, S. A. Reshanov, and H. B. Weber, *Phys. Rev. B* **77**, 155426 (2008).
- [17] G. Kresse and J. Hafner, *Phys. Rev. B* **47**, 558 (1993).
- [18] J.-Y. Veuillen, F. Hiebel, L. Magaud, P. Mallet, and F. Varchon, *J. Phys. D* **43**, 374008 (2010).
- [19] R. Balog, B. Jørgensen, J. Wells, E. Lægsgaard, P. Hofmann, F. Besenbacher, and L. Hornekær, *J. Am. Chem. Soc.* **131**, 8744 (2009).
- [20] D. C. Elias, R. R. Nair, T. M. G. Mohiuddin, S. V. Morozov, P. Blake, M. P. Halsall, A. C. Ferrari, D. W. Boukhvalov, M. I. Katsnelson, A. K. Geim, and K. S. Novoselov, *Science* **323**, 610 (2009).
- [21] S. Ryu, L. Liu, S. Berciaud, Y.-J. Yu, H. Liu, P. Kim, G. W. Flynn, and L. E. Brus, *Nano Lett.* **10**, 4944 (2010).
- [22] J. L. Li, J.-F. Jia, X.-J. Liang, X. Liu, J.-Z. Wang, Q.-K. Xue, Z.-Q. Li, J. S. Tse, Z. Zhang, and S. B. Zhang, *Phys. Rev. Lett.* **88**, 066101 (2002).
- [23] A. T. N'Diaye, S. Bleikamp, P. J. Feibelman, and T. Michely, *Phys. Rev. Lett.* **97**, 215501 (2006).
- [24] M. Caragiu and S. Finberg, *J. Phys. Condens. Matter* **17**, R995 (2005).
- [25] T. von Hofe, J. Kröger, and R. Berndt, *Phys. Rev. B* **73**, 245434 (2006).
- [26] P. A. Khomyakov, *Phys. Rev. B* **82**, 115437 (2010).